International Journal for Modern Trends in Science and Technology
Volume 12, Issue 04, pages 1293-1308
ISSN: 2455-3778 online
Available online at: http://www.ijmtst.com/vol12issue04.html
DOI: https://doi.org/10.5281/zenodo.19697313

Advanced Speed Control of PMSM in EVs Using MPC–ANN with a Single-Inductor Multi-Port Power Converter

Dr.J.Srinu Naick[1] | G. Anusha[2]

[1]*Professor, Dept of EEE, Chadalawada Ramanamma Engineering College, Tirupati, Andhra Pradesh, India*
[2]*PG Student, Dept of EEE, Chadalawada Ramanamma Engineering College, Tirupati, Andhra Pradesh, India*

To Cite this Article
Dr.J.Srinu Naick & G. Anusha (2026). Advanced Speed Control of PMSM in EVs Using MPC–ANN with a Single-Inductor Multi-Port Power Converter. International Journal for Modern Trends in Science and Technology, 12(04), 1293-1308. https://doi.org/10.5281/zenodo.19697313

Article Info
Received: 19 March 2026; Revised: 17 April 2026; Accepted: 20 April 2026.

KEYWORDS

Artificial Neural Network (ANN), Electric Vehicles (EVs), Hybrid Energy Systems, Model Predictive Control (MPC), Multi-Port DC–DC Converter, Permanent Magnet Synchronous Motor (PMSM), Speed Control

ABSTRACT

This paper proposes an isolated single-inductor multi-port DC-DC converter for hybrid energy integration in electric vehicles. The converter has the capability to utilize various types of renewable energy resources, including solar PV and battery storage. Additionally, it provides the ability to control power flow in either direction when charging or discharging. In addition, the proposed converter allows for the generation of multiple output voltage levels to accommodate both high-power traction loads and lower power auxiliary systems found in electric vehicles. Due to its use of a single inductor and thus less components than other converters utilizing multiple inductors, this design represents a more compact and cost effective solution. A number of operating modes were analyzed by developing a model using state space analysis. A proper control scheme was then established that would provide a stable condition of operation regardless of variation in the inputs and/or load. With a multi-level DC output, the proposed converter can be used to interface with the inverter fed electric vehicle drive train thereby providing a reduction in harmonic distortion of the AC output waveforms and better overall drive performance. For enhancement of propulsion performance, a permanent magnet synchronous motor (PMSM) was chosen as the primary load and was operated using a hybrid Model Predictive Control (MPC) and Artificial Neural Network (ANN) based controller. Compared to traditional control schemes, this proposed control method provided superior speed tracking accuracy, minimal steady-state error and greater overall system robustness. Simulations of the entire system were completed using MATLAB/Simulink; these simulations validated the

1. INTRODUCTION

To begin with, the growing global need for energy-efficient and environmentally-friendly means of transportation has driven the world-wide increase in the use of Electric Vehicles (EVs). EVs offer several benefits over traditional internal combustion engines such as; lower green-house gas emission, higher energy efficiency, lower operational costs etc. [1],[2] However, the overall performance and reliability of EV's greatly depends upon the efficiency of the power-conversion and energy-management systems, capable of managing one or more energy sources and/or loads in dynamically changing operating conditions. Recent studies have shown that hybrid energy systems based on combinations of battery-energy-storing elements with renewable-energy-sources such as Solar Photovoltaic (PV) systems will become increasingly important in EV-applications [3],[4]. For example, incorporating solar-energy into EVs may lengthen the "driving-range" of EVs, and reduce the reliance on the electrical-grid for charging. However, hybridizing two energy-sources introduces new complexities associated with the coordination of power-flow among all available energy-source(s), stabilization of the system-voltage-regulation, and optimization of overall system-efficiency [5]. Traditional DC-DC converters were specifically designed for single-input single-output (SISO) operation, thus they cannot efficiently manage simultaneous input from multiple energy sources [6]. To meet these demands, multi-port DC-DC converters have emerged as an attractive option to facilitate the integration of multiple energy-sources and/or loads within a single unified power-conversion platform [7],[8]. Multi-port converters provide bidirectional power-flow capability, fewer conversion stages than SISO converters, and greater overall-system efficiencies. Several configurations exist for multi-port converters however, the single-inductor multi-port converter has received particular attention due to its compact design, smaller part-count, and reduced-cost [9],[10]. Single-inductor multi-port converters utilize a single inductor, thus they may operate in various modes to charge/discharged stored energy-elements at reduced size and increased power-density [11]. Furthermore, most EVs consist of numerous voltage-level requirements to energize various loads including; high power traction-motors, low power auxiliary systems (i.e., lighting, control-units, onboard-electronics), etc. [12]. Thus, multi-port converters able to produce multiple output voltage levels present a viable solution for many EV-related applications. Additionally, multi-port converters may also be effectively connected to multilevel-inverters (MLIs), which are frequently utilized in EV-propulsion systems as MLIs can minimize THD, switching-losses, and torque-ripple in motor-drives [13],[14]. The majority of EVs employ a permanent magnet synchronous motor (PMSM) as the primary source of propulsion due to the motor's high-efficiency, high-power density, and excellent dynamic-performance characteristics [15]; however, precise speed-control of the PMSM is crucial to ensure a smooth and consistent vehicle-operation throughout various loading and driving conditions. Although PI-controllers are widely-employed in motor-controls due to their ease-of-use and simplicity, they possess many disadvantages such as slow-dynamic-responses, large sensitivities-to-parameter-variations, and poor-performance during non-linear operating conditions [16]. To mitigate these drawbacks, advanced motor-control strategies such as model-predictive control (MPC) and artificial neural networks (ANN)-based controllers have recently been investigated. MPC provides rapid dynamic-response and is capable of managing system-constraints therefore making it well-suited for real-time control of PE systems and motor-drives [17]. ANN-based controllers, on the other hand, provide adaptive-learning-capabilities allowing them to optimize performance under non-linear and uncertain operating conditions [18]. The combination of MPC-and-ANN control-strategies presents tremendous opportunity to improve PSM drive-speed-control performance in EV applications. While recent advancements have taken place in multi-port-converters and intelligent-control-methodologies; few investigations have centered around an integrated-design methodology of single-inductor-multiport-converters coupled with hybrid-hybrid control-methodologies for PM-SM driven-EV systems. Existing literature generally focuses on independent designs of either

converter-design or motor-control methodologies without considering the cooperative operation of both sub-systems [19],[20]. Consequently, a comprehensive methodology that integrates efficient power-conversions with intelligent motor-controls is required to improve overall EV performance. In this paper, a novel single-inductor multi-port DC-DC converter for hybrid energy integration in EV applications is presented. The converter is designed to integrate solar-PV and battery-sources while providing multiple-regulated-output-voltages for differing loads. A complete state-space-analysis is conducted to investigate multiple-operating-modes of the converter. Moreover, a PMSM is selected as the principal-load-traction-element in the EV system. Furthermore, a Hybrid-MPC-ANN-controller is developed to provide robust and accurate speed-control of the PMSM [21]-[22]. Lastly, the entire system is fully-modeled and simulated via MATLAB/Simulink software package to validate its performance.

The main contributions of this paper are summarized as follows:

- Design of a single-inductor multi-port DC–DC converter for hybrid energy EV applications
- Development of state-space models for multiple operating modes
- Integration of the converter with a PMSM drive system
- Implementation of a hybrid MPC–ANN controller for improved speed control
- Validation of the proposed system through MATLAB/Simulink simulation

II. Proposed System Configuration

The proposed system contains an integration of a single-inductor multiport DC-DC converter with a voltage source inverter (VSI), which drives a permanent magnet synchronous motor (PMSM) for use in electric vehicles as depicted by Figure 1. The proposed system uses a total of two input supplies. A solar photovoltaic (PV) system provides renewable energy through a diode to prevent backflow; whereas, a battery is connected to the system using controlled switches to provide flexibility in the charging and discharging operation depending upon the load demands and available energy. A single-inductor multiport converter serves as the heart of the proposed system. This type of converter allows for power flow regulation from one or more inputs to one or more outputs utilizing only one inductor, but including multiple switches and diodes. Depending upon the configuration mode, this type of converter is able to produce multiple regulated DC output voltages. In particular, one output will be utilized to sustain the DC-link voltage required for the inverter operation, while another output may be utilized to support auxiliary loads within the vehicle. Due to its low number of components, this type of converter provides the advantages of being small, efficient, and economical. Stabilization of the DC-link voltage is provided through capacitance, thus enabling a smooth and consistent input to the VSI. The VSI transforms the DC voltage to the three phase AC supply that is required for driving the PMSM. The PMSM acts as the primary traction motor for electric vehicles because it has a high level of efficiency and a fast dynamic response. Overall, the proposed system provides flexibility in managing energy. This will allow for optimal usage of both the PV and battery systems so that there will be improved performance and reliability of the electric vehicle.

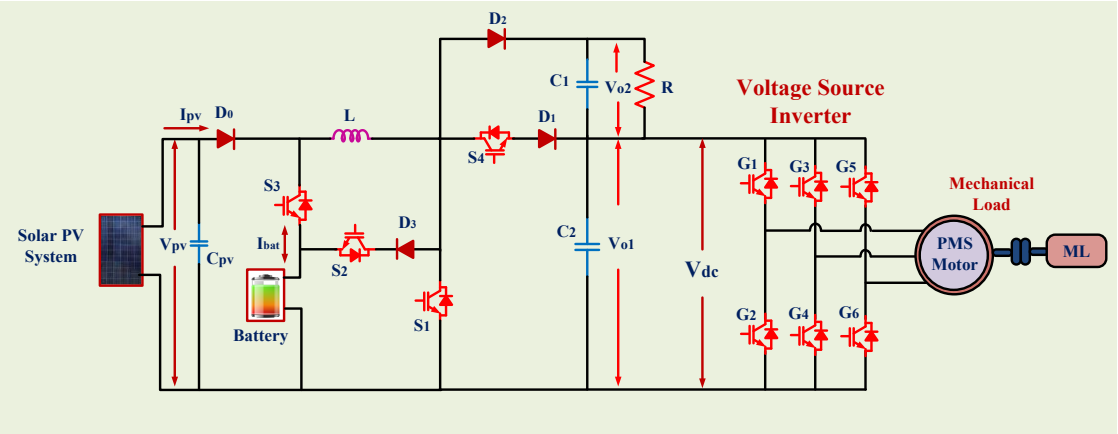

Fig. 1. Proposed multi-port converter with PMSM drive system for EV applications

II. MODELING OF PV ARRAY

To model a solar photovoltaic (PV) panel it is necessary to understand how well a system that incorporates a PV panel will operate. A PV cell uses a semiconductor material to convert photonic (solar) energy into voltaic (electrical) energy. The performance of a PV cell can be modeled by its electrically equivalent circuit which consists of a current source; a diode representing the P-N junction properties of the semiconductor device; and two resistive elements - a series resistance (R_s) and a shunt (parallel) resistance (R_{sh}), as illustrated in Figure 2. The current source is representative of the photocurrent that results from the interaction of sunlight with the surface area of the PV cells. The diode illustrates the P-N junction properties of the semiconductor device. The PV cell's equivalent circuit includes both a series resistance (R_s) and a shunt (or parallel) resistance (R_{sh}). The series resistance accounts for all of the electrical energy lost due to the flow of current through the semiconductor material. Conversely, the shunt resistance is indicative of any electrical energy loss due to leakage within the PV cell.

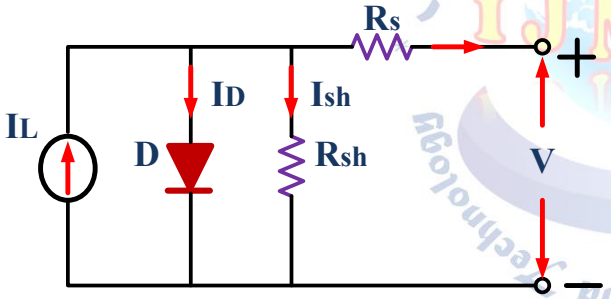

Fig. 2 equivalent model of PV solar.

$$I_{PV} = I_{ph} - I_0\left[\exp\left(\frac{q(V_{PV}+R_sI_{PV})}{N_sAkT}\right) - 1\right] - \frac{V_{PV}+R_sI_{PV}}{N_sR_p} \quad (1)$$

where I_{ph} is the photocurrent that varies depending on solar radiation and temperature; I_0 is the saturation current of the diode; q is the charge of an electron; k is the Boltzmann's constant; T is the temperature of the cell; A is the diode ideality factor. The total number of connected cells is defined by N_s.

The variation of photocurrent due to different irradiances and temperatures has been expressed as:

$$I_{ph} = \left[I_{SC,STC} + K_i(T - T_{STC})\right]\frac{G}{G_{STC}} \quad (2)$$

which indicates how the short-circuit current under standard test conditions (STC) ($I_{SC,STC}$) relates to irradiance (G), temperature (T), solar irradiance at STC (GSTC) and its temperature dependence (K_i). The same considerations apply to the dependence of the diode saturation current on temperature and open circuit voltage parameters.

The output power of the PV array is given by:

$$P_{PV} = V_{PV} \times I_{PV} \quad (3)$$

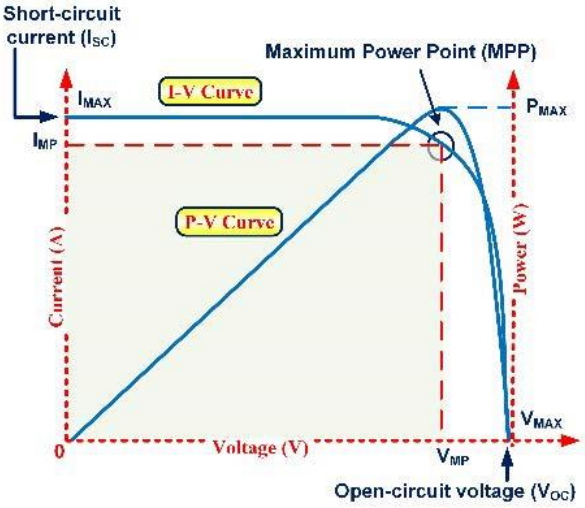

Fig 3. Solar Cell I-V Characteristics

The I-V characteristic of the PV system, as well as the P-V characteristic of the PV system, depend on the irradiance and temperature. The working point of the PV array changes continuously, and there exists a special point called the maximum power point (MPP), where the output power is maximum. The voltage and current values associated with MPP are VMPP and IMPP, respectively as depicted in Fig. 3. Here, a PV module characterized by practical datasheet parameters was modeled using MATLAB/Simulink. To obtain the required voltage and current level, a configuration consisting of series and parallel connections of several PV modules was chosen for the PV array. The developed model captures accurately the non-linear behavior of the PV system when exposed to changing environmental conditions, which makes it suitable for connection to the proposed multiport DC-DC converter.

IV. MODELLING AND DESIGNING OF LITHIUM-ION EV BATTERY

A. Electrochemical Fundamentals

Rechargeable Lithium-Ion Batteries operate via reversible lithium ion insertion (to the cathode), and reversible lithium ion extraction (from the cathode) through reversible chemical oxidation reduction processes where Lithium ions are moved back-and-forth between the Cathodic Transition Metal Oxide electrode and the Graphitic Anode. This enables high efficiencies related to energy storage and release. Because this

process does not result in the formation of Lithium metal on either Electrode it is safer compared to many other rechargeable battery systems and offers longer cycle life. The electrolyte provides for the movement of lithium ions between the cathode and the anode while preventing electron transfer thereby allowing for proper electrochemistry. For each charge and discharge of a Li-ion cell, the overall electrochemical reaction will be represented as [43] [44].

$$Li_xC_6 + Li_{1-x}M_yO_z \rightleftharpoons C_6 + LiM_yO_z \quad (4)$$

where:

- Li_xC_6 represents the lithiated graphite anode,
- $Li_{1-x}M_yO_z$ represents the partially lithiated cathode material,
- M denotes the transition metal (such as Co, Fe, or Mn),
- x represents the degree of lithium intercalation.

Typical cathode materials include lithium cobalt oxide $L_iC_oO_2$), lithium iron phosphate ($L_iF_ePO_4$), and lithium manganese oxide ($L_iMn_2O_4$).

a. Anode Reaction

During the process of charging, Lithium-ions reside within the layer structure of carbon-graphite anodes. During discharge, they exit this storage area. The electrochemical reaction occurring at the anode during discharge is represented below:

$$Li_xC_6 \longrightarrow C_6 + xLi^+ + xe^- \quad (5)$$

The reaction occurs in the reverse direction during the charging process for Lithium-ions to enter the Carbon Graphite Layer Structure.

b. Cathode Reaction

At the Cathode, Lithium-ions are entering the Transition Metal Oxide Structure during Discharge. This Reaction can be expressed as follows:

$$Li_{1-x}M_yO_z + xLi^+ + xe^- \longrightarrow LiM_yO_z \quad (6)$$

During charging, lithium ions are extracted from the cathode material, and the reaction reverses.

B. Battery Modeling and State of Charge Estimation

Although Li-ion Batteries have been utilized in Electric Vehicle Applications for many years now, their advantages; such as High Energy Density, Long Cycle Life and High Efficiency make them ideal candidates for System Level Analysis and Control Design. An accurate Battery Model is necessary for System-Level Analysis and Control Design so that the Electrical Behavior of the Battery can be accurately modeled while varying Operating Conditions. Many Modeling Approaches exist however; the Equivalent Circuit Model (ECM) is one of the most popular models because it offers a compromise between Accuracy and Computational Simplicity (as depicted in Fig.4). The Equivalent Circuit Model represents a battery using an Open-Circuit Voltage Source Voc(SOC),, A Series Internal Resistance R_s, and a Parallel RC Network which accounts for Polarization Effects created by Electrochemical Dynamics. The Open-Circuit Voltage is a Nonlinear Function of State-of-Charge (Soc); The Open-Circuit Voltage represents the internal electrochemical status of a battery.

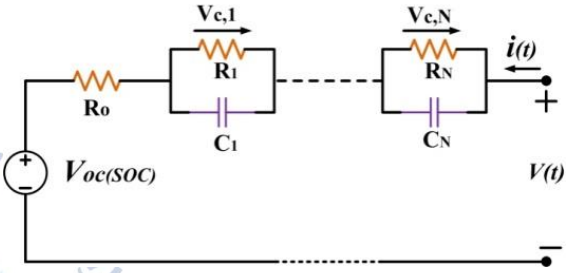

Fig. 4. Equivalent circuit diagram of lithium-ion EV battery

Based on the equivalent circuit, the terminal voltage of the battery can be expressed as

$$V(t) = V_{oc}(SOC) - I(t)R_s - V_{RC}(t) \quad (7)$$

where:

- $V(t)$ is the terminal voltage,
- $V_{oc}(SOC)$ is the open-circuit voltage as a function of SOC,
- $I(t)$ is the battery current (positive during discharge and negative during charge),
- R_s is the internal resistance,
- $V_{RC}(t)$ represents the voltage across the RC polarization network.

The dynamic behavior of the polarization voltage is governed by the first-order differential equation:

$$\frac{dV_{RC}(t)}{dt} = -\frac{1}{R_pC_p}V_{RC}(t) + \frac{1}{c_p}I(t) \quad (8)$$

where R_p and C_p denote the polarization resistance and capacitance, respectively. This RC network captures transient voltage response due to electrochemical processes such as charge transfer and diffusion.

C. State of Charge (SOC) Estimation

The state-of-charge (SOC) determines how much usable energy remains in a battery with respect to its full capacity for storing energy. It is a key factor in most battery-management-systems (BMS). Generally, the SOC will be determined using the Coulomb-counting method. This involves integrating the flow of current into the battery over time.

$$SOC(t) = SOC(0) - \frac{1}{Q_{nom}} \int_0^t I(\tau)\, d\tau \quad (9)$$

where:

- SOC(0) is the initial state of charge,
- Q_{nom} is the nominal battery capacity (Ah),
- I(τ) is the instantaneous current.

For practical implementation, the discrete-time form is given by:

$$SOC(k+1) = SOC(k) - \frac{T_s}{Q_{nom}} I(k) \quad (10)$$

where Ts is the sampling time.

D. Open-Circuit Voltage (OCV–SOC Relationship)

Typically, the open-circuit-voltage (OCV) of a cell is a non-linear function of SOC. However, OCV can be determined experimentally. Approximation techniques have also been developed, and these approximations are often presented in polynomial form or as a lookup table.

$$V_{oc}(SOC) = a_0 + a_1 SOC + a_2 SOC^2 + \ldots + a_n SOC^m \quad (11)$$

An accurate model of the open-circuit voltage will be needed to predict voltages with good accuracy and to estimate battery state with sufficient accuracy.

V. PROPOSED DC-DC CONVERTER

The proposed system uses a single-inductor multiport dc-dc converter to couple a solar photovoltaic (PV) source and a battery to supply an electric vehicle application. The converter includes one inductor L, four switches S1-S4, four diodes D1-D4, and two capacitors (C_1, C_2). Outputs of the converter include the DC link that supplies the inverter and auxiliary loads (V_1, V_2). The most important feature of this configuration is the use of a single inductor to control three different paths of current flow into and out of the output ports of the converter. This configuration reduces the number of components in the circuit to improve efficiency as illustrated in Fig.5. Operation of the dc-dc converter is determined by both the ability to store energy in the inductor during time it is conducting at the input port and its ability to release stored energy to the output ports through the capacitors' regulation of voltage.

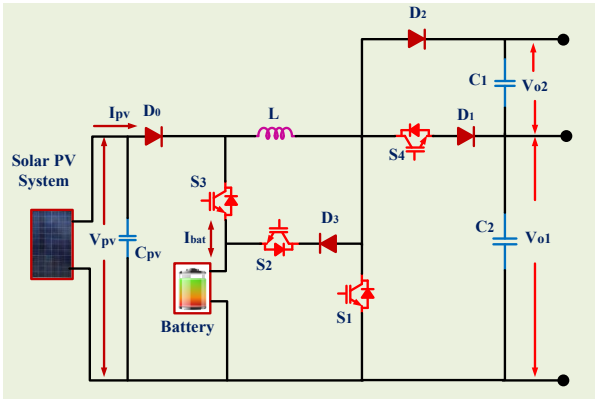

Fig.5 Proposed single-inductor multi-port DC–DC converter for PV–battery integrated electric vehicle system.

$$L\frac{di_L}{dt} = V_L \quad (12)$$

V_L is the instantaneous voltage across the inductor. The output capacitors regulate the voltage levels so as to compensate for differences between inductor current and load current as described by the following equations:

$$C_1\frac{dV_1}{dt} = i_L - \frac{V_1}{R_1} \quad (13)$$

$$C_2\frac{dV_2}{dt} = i_L - \frac{V_2}{R_2} \quad (14)$$

These equations show that when the inductor current supplies a larger amount than needed by the load, then the capacitors are being charged. Conversely, if the load requires more current than what is supplied by the inductor current, then the capacitors discharge to ensure continuous voltage. Based upon the availability of solar energy and the load requirements, there are two operating modes for the converter; battery charging and battery discharging. In each mode, there are several periods of time during which the switches turn ON/OFF to allow or restrict flow of energy throughout the converter.

A. BATTERY DISCHARGING MODE

When in this mode, both input sources V_{pv} and V_{bat} are providing power to the load. The switches S_1, S_3 and S_4 are active. Switches S_2 is de-activated. The converter has an operating point that falls in a continuous conduction mode (CCM). This ensures a smooth inductor current with low ripple. Within every switching cycle, all activities occur at four points of time referred to as switching states as follows.

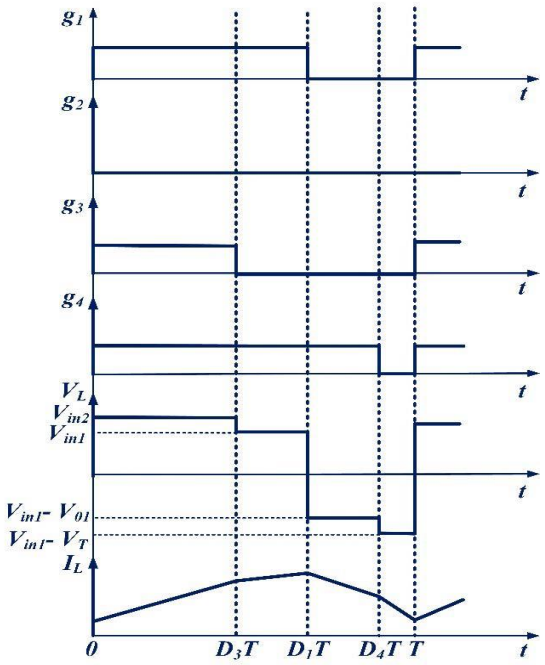

Fig.6. Typical steady-state waveform while discharging a battery

1) SWITCHING CONDITION 1 (0<t<D3T)

This interval is characterized by two switched on (S_1) & (S_3). The PV is connected to the Inductor. It will begin to store energy and cause an increased linear rise in the Inductor Current. Since the load does not receive any energy from the inductor during this time frame, the load requirement will be supplied by capacitors C_1 & C_2. Both capacitors will have discharged and caused a gradual decline in the output voltages.

$$L\frac{di_L}{dt} = V_{pv} \quad (15)$$

$$C_1\frac{dV_1}{dt} = -\frac{V_1}{R_1} \quad (16)$$

$$C_2\frac{dV_2}{dt} = -\frac{V_2}{R_2} \quad (17)$$

2) SWITCHING CONDITION 2 (D3T<t<D1T)

The same thing happens again. Switches S_1 & S_3 are still operating. The inductor continues to collect energy from the PV Source and increase its current further. Capacitors continue to discharge to provide continuous power to the load. In addition, the inductors' ability to store energy will allow for subsequent energy transfers to the outputs.

$$L\frac{di_L}{dt} = V_{pv} \quad (18)$$

$$C_1\frac{dV_1}{dt} = -\frac{V_1}{R_1} \quad (19)$$

$$C_2\frac{dV_2}{dt} = -\frac{V_2}{R_2} \quad (20)$$

3) SWITCHING CONDITION 3 (D1T<t<D4T)

Switches S_1 & S_3 remain closed but S_4 has been opened. The energy stored in the inductor was transferred to the first output V_1. The inductor's current decreased after being transferred. Capacitor C_1 was charged with the inductor current that caused an increase in its voltage; and at the same time, capacitor C_2 continued to discharge and supply the load.

$$L\frac{di_L}{dt} = V_{pv} - V_1 \quad (21)$$

$$C_1\frac{dV_1}{dt} = i_L - \frac{V_1}{R_1} \quad (22)$$

$$C_2\frac{dV_2}{dt} = -\frac{V_2}{R_2} \quad (23)$$

4) SWITCHING CONDITION 4 (D4T<t<T)

Finally, the last interval. All of the switches were turned off. Energy is being released by the inductor into both output capacitors via the diodes. The inductor's current decreased further because it is providing energy to both outputs. At this point, both capacitors are being charged, restoring their voltage levels and stabilizing the output voltages.

$$L\frac{di_L}{dt} = V_{pv} - (V_1 + V_2) \quad (24)$$

$$C_1\frac{dV_1}{dt} = i_L - \frac{V_1}{R_1} \quad (25)$$

$$C_2\frac{dV_2}{dt} = i_L - \frac{V_2}{R_2} \quad (26)$$

B. BATTERY CHARGING MODE

When using MPPT Mode, the PV Source provides power to the load and also charges the Battery. Switches S1, S2 and S4 are On, while switch S3 is Off. In addition, depending upon load conditions, the Converter can work in Discontinuous Conduction Mode (DCM) or Continuous Conduction Mode. The operation of the Converter is defined over four time intervals.

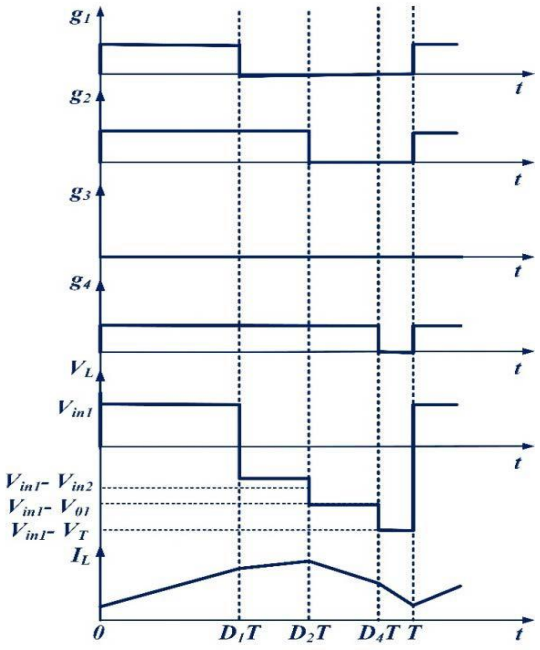

Fig.7 The typical steady-state waveform in the charging mode of a battery

1) SWITCHING CONDITION 1 (0<t<D1T)

Switch S1 is on; Energy is supplied from the PV Source to charge the Inductor. The Current through the Inductor increases as it stores energy. Because the Inductor has not started supplying energy to the Load, the two Output Capacitors continue to provide a path for the load's energy requirements.

$$L\frac{di_L}{dt} = V_{pv} \quad (27)$$

$$C_1\frac{dV_1}{dt} = -\frac{V_1}{R_1} \quad (28)$$

$$C_2\frac{dV_2}{dt} = -\frac{V_2}{R_2} \quad (29)$$

2) SWITCHING CONDITION 2 (D1T<t<D2T)

Switch S2 is turned On. The Stored Energy in the Inductor is now being transferred to the Battery at a controlled rate. The Current flowing through the Inductor is decreasing because the Battery Voltage opposes that of the PV Source. The two Output Capacitors continue to supply energy to the load.

$$L\frac{di_L}{dt} = V_{pv} - V_{bat} \quad (30)$$

$$C_1\frac{dV_1}{dt} = -\frac{V_1}{R_1} \quad (31)$$

$$C_2\frac{dV_2}{dt} = -\frac{V_2}{R_2} \quad (32)$$

3) SWITCHING CONDITION 3 (D2T<t<D4T)

Switch S4 is turned On. The Inductor transmits its stored energy to the First Output. At the same time, Capacitor C1 begins to receive the flow of energy from the Inductor Current. The second Output Capacitor C2 continues to transfer energy to the load.

$$L\frac{di_L}{dt} = V_{pv} - V_1 \quad (33)$$

$$C_1\frac{dV_1}{dt} = i_L - \frac{V_1}{R_1} \quad (34)$$

$$C_2\frac{dV_2}{dt} = -\frac{V_2}{R_2} \quad (35)$$

4) SWITCHING CONDITION 4 (D4T<t<T)

All of the Switches are turned Off. The stored energy within the Inductor is released to both Outputs simultaneously via the Diodes. Both Output Capacitors are being charged during this time period so they can maintain their required voltages and ensure good output stability and performance.

$$L\frac{di_L}{dt} = V_{pv} - (V_1 + V_2) \quad (36)$$

$$C_1\frac{dV_1}{dt} = i_L - \frac{V_1}{R_1} \quad (37)$$

$$C_2\frac{dV_2}{dt} = i_L - \frac{V_2}{R_2} \quad (38)$$

VI. PMSM MODELING

The main traction motor in the proposed electric vehicle system is a permanent magnet synchronous motor (PMSM), which is connected via an inverter with a three phase VSI. The DC-link voltage that feeds the inverter is provided from the multi-port DC-DC converter. The inverter then takes this regulated DC voltage and provides it as a controllable three-phase AC voltage at the stator windings of the PMSM. As there is no need to provide an external excitation due to the permanent magnets on the rotor, the PMSM has a higher efficiency than other motors and also better power density. To enable an accurate model and control design for the PMSM, the PMSM is represented in the rotating d-q reference frame by use of Park's transformation. By transforming the three-phase system to the d-q coordinate system by Park's transformation, we can simplify the representation of the three-phase system to two orthogonal systems, thus allowing us to easily control both flux and torque.

$$v_d = R_s i_d + L_d\frac{di_d}{dt} - \omega_e L_q i_q \quad (39)$$

$$v_q = R_s i_q + L_q\frac{di_q}{dt} + \omega_e L_d i_d + \omega_e \lambda_f \quad (40)$$

where v_d and v_q are the stator voltages, i_d and i_q are the stator currents, R_s is the stator resistance, L_d and L_q are the inductances, ω_e is the electrical speed, and λ_f is the flux linkage due to the permanent magnets.

From these equations, the current dynamics can be expressed as

$$\frac{di_d}{dt} = \frac{1}{L_d}\left(v_d - R_s i_d + \omega_e L_q i_q\right) \quad (41)$$

$$\frac{di_q}{dt} = \frac{1}{L_q}\left(v_q - R_s i_q - \omega_e L_d i_d - \omega_e \lambda_f\right) \quad (42)$$

The electromagnetic torque developed by the PMSM is given by

$$T_e = \frac{3}{2}\frac{P}{2}\left[\lambda_f i_q + \left(L_d - L_q\right) i_d i_q\right] \quad (43)$$

For surface-mounted PMSM, Ld≈Lq, and hence the torque equation simplifies to

$$T_e = \frac{3}{2}\frac{P}{2}\lambda_f i_q \quad (44)$$

This indicates that the torque is primarily controlled by the q-axis current, while the d-axis current is maintained near zero for maximum torque per ampere operation.

The mechanical dynamics of the PMSM are governed by

$$T_e - T_L = J\frac{d\omega_m}{dt} + B\omega_m \quad (45)$$

where T_L is the load torque, J is the inertia, B is the friction coefficient, and ω_m is the mechanical speed. The relation between electrical and mechanical speed is given by

$$\omega_e = \frac{P}{2}\omega_m \quad (46)$$

VSI for pmsm drive operation

VII. DRIVING MODE CONTROL STRATEGY

A. Driving Mode of Voltage Source Inverter (VSI)

The main traction motor for this proposed electrical vehicle system is a Permanent Magnet Synchronous Motor (PMSM), as seen in Figure 8. A Three-Phase Voltage Source Inverter (VSI) interfaces with the PMSM. The VSI takes the regulated DC link voltage from the multi-port DC-DC converter and converts it into controlled three phase AC voltages that drive the stator winding of the PMSM. Because there are no external excitations provided to the rotor due to the presence of permanent magnets within the rotor, the PMSM has a higher efficiency than other motors and greater power density. To accurately model and develop controls for the PMSM, it is analyzed in the rotating d-q reference frame, which uses Park's Transformation. By transforming the three-phase system into two perpendicular components, this enables simpler control over flux and torque.

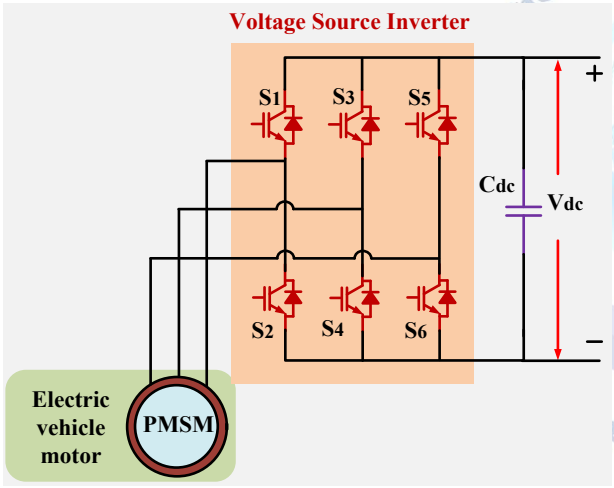

Fig.8 Electric Vehicle Drive System Using VSI-Fed PMSM

The phase voltages with respect to the DC-link midpoint are given by

$$v_a = \frac{V_{dc}}{2}(S_1 - S_2) \quad (47)$$

$$v_b = \frac{V_{dc}}{2}(S_3 - S_4) \quad (48)$$

$$v_c = \frac{V_{dc}}{2}(S_5 - S_6) \quad (49)$$

where Si∈{0,1} denotes the switching state of each device. The corresponding line-to-line voltages are expressed as

$$v_{ab} = v_a - v_b \quad (50)$$

$$v_{bc} = v_b - v_c \quad (51)$$

$$v_{ac} = v_c - v_a \quad (52)$$

The inverter switching signals are generated using pulse-width modulation (PWM), where the reference voltages are compared with a high-frequency carrier signal:

$$S(t) = \begin{cases} 1, & v_{ref}(t) > V_{carrier}(t) \\ 0, & v_{ref}(t) \le V_{carrier}(t) \end{cases} \quad (53)$$

This modulation ensures the generation of sinusoidal output voltages with controlled amplitude and frequency. During driving mode, the energy flow path is Multi-source inputs (Battery/solar) → Multi-Port DAB Converter → DC-Link → VSI → PMSM

The multi-port DAB converter regulates DC link voltage and manages the flow of electrical energy from the various ports (energy sources). The VSI adjusts the voltage, current, and frequency to regulate motor operation. The VSI adjusts the electromagnetic torque as a function of current to ensure that the motor accelerates smoothly and efficiently. The VSI based driving mode allows for an efficient conversion of DC energy to controlled AC power for the PMSM. The combination of the VSI driving mode with the multi-port DAB converter will provide a stable DC link voltage and allow for effective energy management while the inverter will allow for precise control over both speed and torque of the motor, making it ideal for high performance electric vehicle propulsion systems.

B. Proposed Model Predictive Control Scheme for PMSM Speed Regulation

In the driving mode, the PMSM's speed is controlled through a Model Predictive Control (MPC) strategy which is illustrated in Figure 9. The proposed control method consists of an Artificial Neural Network (ANN)-speed loop along with Finite Control Set Model Predictive Controller (FCS-MPC) for inverter switching. The ANN block processes the speed error and produces the reference q-axis current $i_{q,ref}$. The d-axis reference current was set to 0, or $i_{d,ref}$ = 0 so that it will have decoupled torque and higher efficiency. The measured three phase stator currents are converted from abc to dq reference frame through the rotor electrical angle θ, and the resultant d and q components are then provided to the MPC block to simulate the future current behaviors and select the best possible voltage source inverter switching states.

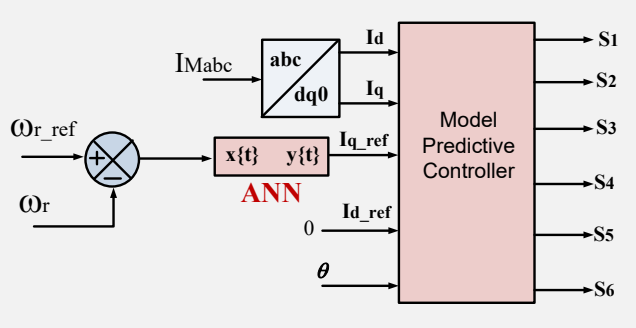

Fig.9 ANN-Assisted Model Predictive Control Scheme for PMSM Speed Regulation

The speed error is first obtained as

$$e_\omega(k) = \omega_{r,ref}(k) - \omega_r(k) \quad (54)$$

where $\omega_{r,ref}$ is the reference rotor speed and ω_r is the measured rotor speed. The ANN controller uses this error to generate the torque-producing current reference, which can be written as

$$i_{q,ref}(k) = ANN\big(e_\omega(k), \Delta e_\omega(k)\big) \quad (55)$$

where $\Delta e_\omega(k)$ denotes the variation in speed error. Since surface-mounted PMSM operation generally adopts zero d-axis current control, the reference d-axis current is selected as

$$i_{d,ref}(k) = 0 \quad (56)$$

The measured three-phase currents are transformed into the rotating reference frame through Clarke–Park transformation. The stator voltage equations of the PMSM in the synchronous dq-frame are expressed as

$$v_d = Ri_d + L\frac{di_d}{dt} - \omega_e L i_q \quad (57)$$

$$v_q = Ri_q + L\frac{di_q}{dt} - \omega_e L i_d + \omega_e \psi_f \quad (58)$$

where R is the stator resistance, L is the stator inductance, ω_e is the electrical angular speed, and ψ_f is the permanent magnet flux linkage. In the implemented predictive controller, the system model is discretized using the forward Euler approximation with sampling time Ts. Thus, the predicted d-axis and q-axis currents for the next sampling instant are obtained as

$$i_d(k+1) = \left(1 - \frac{RT_s}{L}\right) i_d(k) + T_s i_q(k) + \frac{T_s}{L} v_d(k) \quad (59)$$

$$i_q(k+1) = \left(1 - \frac{RT_s}{L}\right) i_q(k) + T_s i_d(k) - \psi_f T_s + \frac{T_s}{L} v_q(k) \quad (60)$$

The MPC algorithm evaluates all possible switching states of the two-level three-phase inverter. Since the inverter has eight possible switching combinations, the candidate switching set is defined as

$$S = \{000, 001, 010, 011, 100, 101, 110, 111\}$$

For each switching state, the inverter phase voltages are calculated as

$$V_{inva} = \frac{V_{dc}}{3}(2S_a - S_b - S_c) \quad (61)$$

$$V_{invb} = \frac{V_{dc}}{3}(2S_b - S_a - S_c) \quad (62)$$

$$V_{invc} = \frac{V_{dc}}{3}(2S_c - S_a - S_b) \quad (63)$$

where V_{dc} is the DC-link voltage and S_a, S_b, and S_c are the switching states of the three inverter legs. These voltages are then transformed into the synchronous reference frame using the rotor position angle θ as

$$v_q = \frac{2}{3}\left[V_{inva}\cos\theta + V_{invb}\cos\left(\theta - \frac{2\pi}{3}\right) + V_{invc}\cos\left(\theta + \frac{2\pi}{3}\right)\right] \quad (64)$$

$$v_d = \frac{2}{3}\left[V_{inva}\sin\theta + V_{invb}\sin\left(\theta - \frac{2\pi}{3}\right) + V_{invc}\sin\left(\theta + \frac{2\pi}{3}\right)\right] \quad (65)$$

Using these predicted voltages, the future current values $i_d(k+1)$ and $i_q(k+1)$ are estimated for each switching state. A quadratic cost function is then formulated to quantify the tracking error between the predicted currents and their reference values:

$$J_i = \left(i_{d,ref} - i_d(k+1)\right)^2 + \left(i_{q,ref} - i_q(k+1)\right)^2 \quad (66)$$

The optimal switching state is selected as the one that minimizes the cost function, namely

$$S_{opt} = arg\min J_i \quad (67)$$

After identifying the optimal switching vector, the corresponding gate pulse pattern is applied to the inverter switches S1–S6. The switching table implemented in the MATLAB function maps the selected state directly to the inverter gating sequence. In this way, the controller avoids the use of a separate PWM modulator and directly generates the optimal switching pulses at each sampling instant. The main advantage of the proposed ANN-assisted MPC scheme is that it combines the fast dynamic response of predictive control with the nonlinear approximation capability of ANN. The ANN provides an adaptive reference current command for speed regulation, while the MPC ensures accurate current tracking by selecting the best inverter switching state based on the discrete motor model. This approach improves speed response, reduces steady-state error, and enhances the overall drive performance of the PMSM under varying operating conditions. For completeness, the electromagnetic torque of the PMSM can be expressed as

$$T_e = \frac{3}{2} p \psi_f i_q \quad (68)$$

for the case $i_d = 0$ (where p denotes the number of pole-pairs), shows that the motor-torque can be directly regulated using the q-axis current; hence the ANN

generated i_{qref} serves as a basis for determining the speed-control output. In summary, the proposed MPC methodology enables an efficient and precise PMSM speed control during driving mode by integrating ANN based reference generation with a FCS-PPC based on current control. The methodology has particular relevance to EVs due to its rapid response, reduced complexity regarding the evaluation of switching-states, and ability to effectively manage the non-linear characteristics associated with the PMSM drive system.

VIII. ARTIFICIAL NEURAL NETWORK (ANN) CONTROLLER DESIGN

In the proposed control strategy, a controller based on an artificial neural network (ANN) will be used to control the two output voltages from the Single-Inductor Multi-Output Converter (SIMOC), and to control the speed of the permanent magnet synchronous machine (PMSM). The SIMOC in the proposed Electric Vehicle System produces two output voltages, i.e., V_{o1} and V_{o2}. On the other hand, the PMSM is considered as the primary traction load. Hence, the controller is expected to carry out three important control tasks: Control of the First Output Voltage; Control of the Second Output Voltage; and Speed Control of PMSM. A Multi-Objective Control Structure is implemented that would improve the performance of the whole system by allowing fast dynamics in transient responses, lower steady state errors, and better stability when there are changes in the source or load.

The ANN controller has replaced the traditional PI controller and can act as a non-linear mapping function between the error signals and the corresponding control signals. Due to its ability to adapt itself during various nonlinear working conditions and parameter variations/uncertainties, ANN is very suitable for application in this type of converters which have multiple switching modes. Thus, the ANN continuously evaluates the desired and actual values of V_{o1}, V_{o2}, and the PMSM's speed, then determines the proper duty cycle or control signal needed for operation of both the converter and inverter.

A. Control Inputs and Error Signals

To simultaneously control the PMSM's speed and the output voltages, the ANN has to be fed the error signals for each regulated variable; specifically, the voltage error will be defined as:

$$e_1(k) = V_{o1,ref}(k) - V_{o1}(k) \quad (69)$$

$$e_2(k) = V_{o2,ref}(k) - V_{o2}(k) \quad (70)$$

and the speed error is defined as

$$e_\omega(k) = \omega_{ref}(k) - \omega_m(k) \quad (71)$$

The corresponding change in error terms are given by

$$\Delta e_1(k) = e_1(k) - e_1(k-1) \quad (72)$$

$$\Delta e_2(k) = e_2(k) - e_2(k-1) \quad (73)$$

$$\Delta e_\omega(k) = e_\omega(k) - e_\omega(k-1) \quad (82)$$

Thus, the complete input vector to the ANN can be written as

$$x(k) = [e_1(k), \Delta e_1(k), e_2(k), \Delta e_2(k), e_\omega(k), \Delta e_\omega(k)] \quad (74)$$

This input vector enables the ANN to learn the combined effect of converter output regulation and motor speed control.

B. ANN Structure

The ANN model employed in this work was a three-layered Feed Forward Neural Network (ANN) with one input layer, multiple hidden layers and an output layer as depicted by Fig.10. The first layer processes the input values and their error values, then passes the results through the second and third layers which contain the nonlinear relationships between the input variables and the output variables. Finally, the last layer produces the control signal. In mathematical terms, the ANN output can be expressed as:

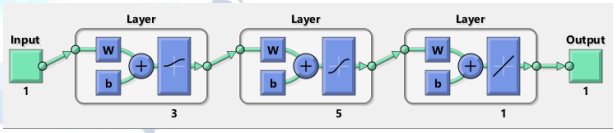

Fig 10: Structure of Neural Network

$$u(k) = [u_1(k), u_2(k), u_3(k)] \quad (75)$$

where $u_1(k)$, $u_2(k)$, and $u_3(k)$ are the control signals corresponding to V_{o1}, V_{o2}, and PMSM speed control, respectively.

Each neuron computes a weighted sum of its inputs as

$$v_j = \sum_{i=1}^{n} \omega_{ji} x_i + b_j \quad (76)$$

where w_{ji} is the weight between the i^{th} input and the j^{th} neuron, and b_j is the bias term. The neuron output is then obtained through an activation function:

$$y_j = f(v_j) \quad (77)$$

In addition, the output layer contains a linear activation function whereas the hidden layer(s) employ either a Sigmoid function or Hyperbolic Tangent function.

C. Forward Computation

The forward propagation of the ANN is expressed as

$$h_1 = f_1(w_1 x + b_1) \quad (78)$$

$$h_1 = f_1(w_2 h_1 + b_2) \quad (79)$$

$$u(k) = w_3 h_2 + b_3 \quad (80)$$

where w_1, w_2, and w_3 are the weight matrices of the respective layers, and b_1, b_2, and b_3 are the bias vectors.

The control outputs are used as follows:

- $u_1(k)$ regulates the first output voltage V_{o1}
- $u_2(k)$ regulates the second output voltage V_{o2}
- $u_3(k)$ regulates the PMSM speed through inverter control

D. Control Law for Three Operations

The ANN-based control law for the three operations is written as

$$u_1(k) = ANN_1\big(e_1(k), \Delta e_1(k)\big) \quad (81)$$

$$u_2(k) = ANN_2\big(e_2(k), \Delta e_2(k)\big) \quad (82)$$

$$u_3(k) = ANN_3\big(e_\omega(k), \Delta e_\omega(k)\big) \quad (83)$$

or in combined form,

$$[u_1(k), u_2(k), u_3(k)] = ANN\big[e_1, \Delta e_1, e_2, \Delta e_2, e_\omega, \Delta e_\omega\big] \quad (84)$$

V_{o1} and V_{o2}. (the first two) are utilized as a means of regulating the duty cycle of the converters; whereas, the third is for PMSM speed control via a voltage source inverter.

If the control outputs are directly interpreted as duty ratios or modulation indices, then

$$D_1(k) = u_1(k) \quad (85)$$

$$D_2(k) = u_2(k) \quad (86)$$

and the speed control signal can be expressed as

$$m(k) = u_3(k) \quad (87)$$

where $D_1(k)$ and $D_2(k)$ are the duty cycles for converter voltage regulation, and $m(k)$ is the modulation or reference signal used for inverter switching.

E. Regulation of Vo1

The first control objective is to regulate V_{o1}. The ANN compares V_{o1}ref to V_{o1} and sends an appropriate control signal to increase or decrease the duty ratio based on the voltage error. If V_{o1} falls below its reference level, the ANN will send a control signal that will allow more power to be delivered by the inductor to V_{o1} capacitor to maintain the desired level. Conversely, if V_{o1} is greater than the reference, the ANN will reduce the duty ratio to ensure voltage regulation. Thus, the controller for the first output is governed by

$$e_1(k) = V_{o1,ref}(k) - V_{o1}(k) \quad (88)$$

$$u_1(k) = ANN_1\big(e_1(k), \Delta e_1(k)\big) \quad (89)$$

F. Regulation of Vo2

The second control objective is to regulate V_{o2}. In like fashion to the first objective, the ANN utilizes the change in voltage error to produce the proper control signal. Therefore, regardless of whether there has been a dynamic change in the load connected to V_{o2}, this output maintains a stable state.

The regulation equations are

$$e_2(k) = V_{o2,ref}(k) - V_{o2}(k) \quad (90)$$

$$u_2(k) = ANN_2\big(e_2(k), \Delta e_2(k)\big) \quad (91)$$

This control action maintains the required auxiliary voltage level.

G. PMSM Speed Control

The third goal of control objectives is speed control for a Permanent Magnet Synchronous Motor (PMSM). A comparison is made of the reference speed of the motor with the actual speed, creating an error. This error is then used by the ANN as the basis of producing a control signal to be sent to the inverter to allow it to operate.

The speed error is given by

$$e_\omega(k) = \omega_{ref}(k) - \omega_m(k) \quad (92)$$

and the control law is

$$u_3(k) = ANN_3\big(e_\omega(k), \Delta e_\omega(k)\big) \quad (93)$$

The PMSM electromagnetic torque is mainly controlled through the q-axis current, which is related to speed control as

$$T_e = \frac{3}{2}\frac{P}{2}\lambda_f i_q \quad (94)$$

Thus, the ANN speed controller indirectly adjusts the inverter output so that the required q-axis current is obtained, ensuring accurate speed tracking.

H. Working of the Proposed Three-Operation Controller

In addition to controlling the two output voltages of the converter during operation, the ANN also controls the speed of the PMSM. At each time interval k, the ANN compares the two output voltages of the inverter with their respective reference values and modifies the input signals $u_1(k)$ and $u_2(k)$, respectively, to maintain regulation of both V_{o1} and V_{o2}. Likewise, at each time interval k, the ANN compares the desired speed of the PMSM with its actual speed and modifies the input signal $u_3(k)$ to produce sufficient voltage and/or current through the inverter to maintain the desired speed.

I. Performance Function and Training

The ANN is trained by minimizing the performance index defined as

$$E = \frac{1}{2}\sum_{k=1}^{N}\Big[\big(d_1(k) - y_1(k)\big)^2 + \Big(\big(d_2(k) - y_2(k)\big)\Big)^2 + \Big(\big(d_3(k) - y_3(k)\big)\Big)^2\Big] \quad (95)$$

where $d_1(k)$, $d_2(k)$, and $d_3(k)$ are the desired control outputs, and $y_1(k)$, $y_2(k)$, and $y_3(k)$ are the ANN outputs. The weights are updated iteratively to reduce the total error and improve controller accuracy.

IX. SIMULATION RESULTS AND DISCUSSION

A. Performance Evaluation of the Multi-Port DC-DC Converter Fed PMSM Drive

The proposed single-inductor multi-output DC-DC converter that integrates a voltage source inverter fed permanent magnet synchronous machine drive was simulated on MATLAB/Simulink to assess its steady-state and dynamic behavior. The simulations showed that the proposed DC-DC converter has been able to provide excellent voltage regulation; proper power distribution among the PV source and battery; and correct PM-SMC speed regulation via the artificial neural network (ANN) controller as described in. The PV source characteristics indicate that although the PV voltage is maintained nearly constant, the PV current and therefore power vary according to the operational conditions. At first, the PV current is about 39 A, resulting in approximately 4.2 kW of power produced. However, as the operational conditions change, the PV current diminishes stepwise to produce less power. For instance, between 0.6 s and 0.8 s, the PV power approaches zero due to decreased availability from the PV source. Following this period of limited PV power production, the PV current begins increasing once more to regain some of the lost power as indicated in Figure 11. These simulation results illustrate that the proposed system is capable of functioning properly when subjected to variable levels of solar radiation. The battery's performance is indicative of proper bidirectional exchange of electrical power. Both positive and negative values for battery current indicate whether energy is being supplied or consumed. When low levels of power are being generated by the PV module, the battery supplies energy to the load. Conversely, when high levels of electrical power are available from the PV module, the battery is charged. Battery voltage remained relatively stable at 86-88 V. Additionally, the SOC varied very little, illustrating the proposed system's ability to manage energy balance as demonstrated in Figure 12. The proposed DC-DC converter's output voltages exhibit excellent regulation performance. The total DC-link voltage (V_T) achieved its desired value of 600 V almost instantaneously and remained there. This is sufficient for use as input to an inverter. Output voltages (V_{o1} and V_{o2}) were established at their respective desired values of 500 V and 100 V with negligible ripple. Thus, it can be concluded that the proposed DC-DC converter successfully regulates multiple outputs simultaneously as illustrated in Figure 13. In addition to demonstrating good regulation performance, the proposed DC-DC converter's PMSM drive performance illustrates rapid dynamic response. The motor quickly reached its desired speed of 2000 RPM and maintained it with negligible steady-state error. Motor torque exhibited an initial transient peak to facilitate acceleration of the motor. Once accelerated, torque stabilized at a steady value as depicted in Figure 14. Stator currents were well-balanced and sinusoidal, thus verifying that the inverter functioned correctly. Comparing PI and ANN controllers revealed that the ANN controller provided significantly improved performance than the PI controller. While the PI controller exhibited increased overshoot and longer settling times, the ANN controller had shorter settling times and smaller oscillations. Also, when transitioning speeds, the ANN controller tracked references more accurately and provided greater stability as illustrated in Figure 14. Therefore, overall, the simulation results verified that proposed system efficiently manages electrical power; provides stable voltage regulation; and precisely controls PMSM speed. Furthermore, the ANN controller dramatically improves upon the dynamic performance relative to the conventional PI controller and allows for successful application of the proposed system to electric vehicles.

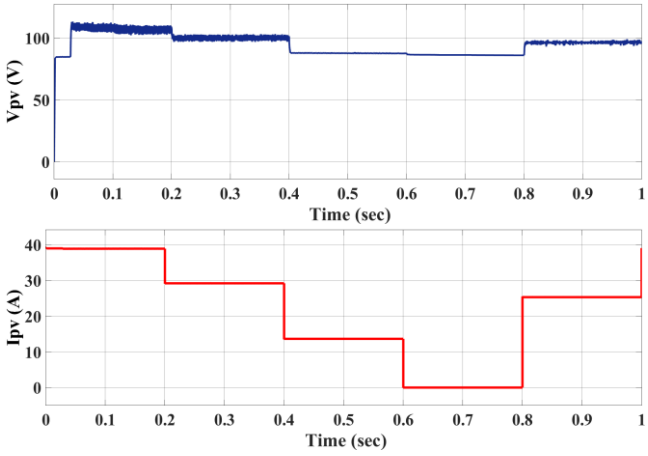

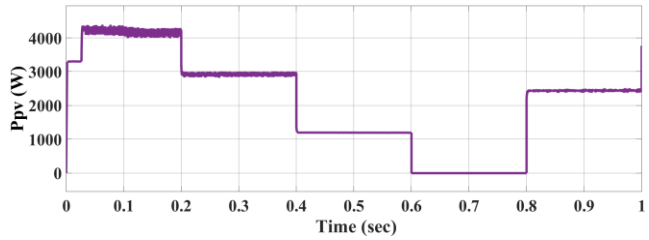

Fig. 11. PV voltage, current, and power characteristics

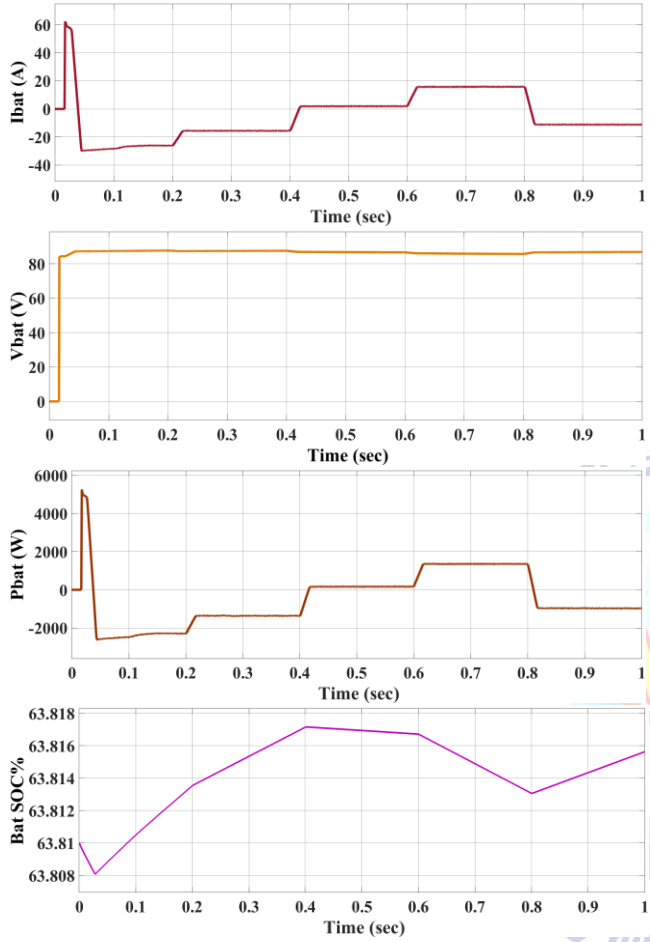

Fig. 12. Battery current, voltage, power and state of charge characteristics

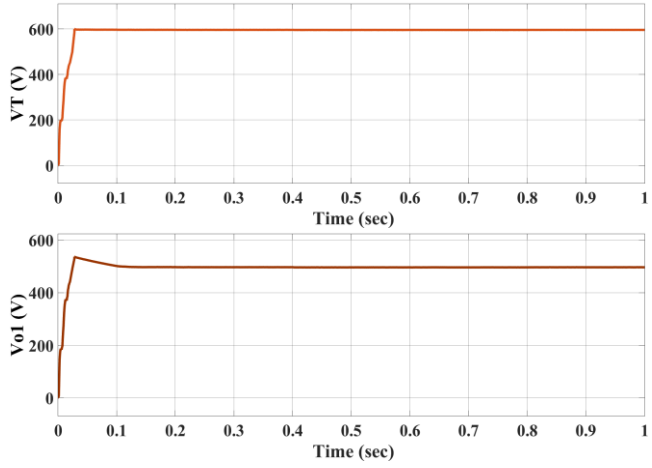

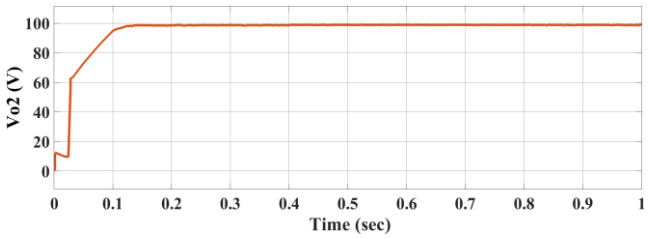

Fig. 13. Converter output voltages response

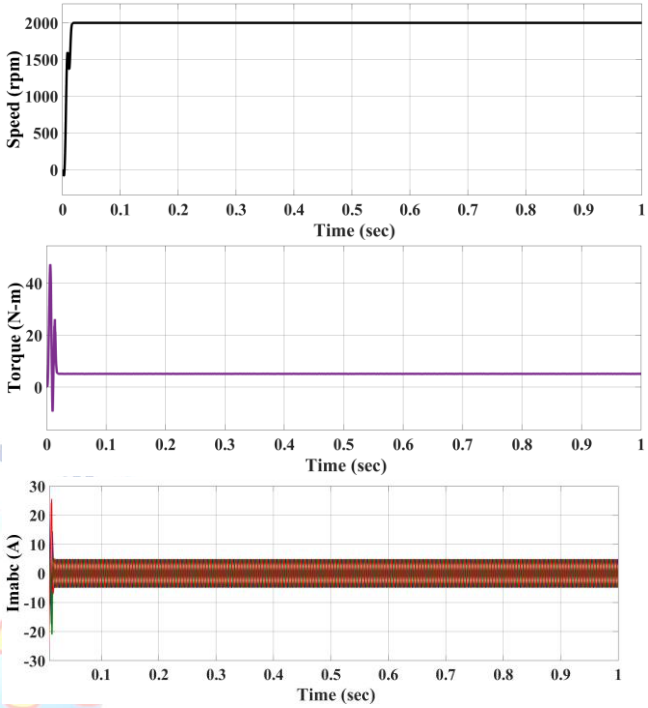

Fig. 14. PMSM torque, phase current, and speed response

B. Performance Evaluation of PI and ANN Controllers

Fig. 13 compares the PI and ANN controllers based on their performances of the speed response and electromagnetic torque of the PMSM. As can be seen from the speed response, both controllers were able to track the reference speed. At first (0–0.2s) however the PI controller had a large amount of overshoot as it reached about 2500rpm before slowly coming back down to the reference speed of 2000rpm. By comparison, the ANN controller followed the reference speed with little or no overshoot and was able to settle back to the reference speed much quicker than the PI controller. This clearly indicates an improvement in transient response of the ANN controller as well as an improvement in stability when compared to the PI controller. When additional step changes were applied to the speed of the motor (around 0.2s, 0.4s, 0.6s and 0.8s), both controllers were able to track the reference profile but once again the PI controller showed a larger amount of under shoot after each step decrease in speed and a longer settling time. Conversely, the ANN controller maintained a tighter

tracking of the reference profile with very small deviations and a much shorter settling time to adjust to the new condition. Once again this indicates the ability of the ANN controller to adjust to new or dynamic operating conditions. The performance difference is also evident from the torque response of the motors. The PI controller produced a number of large negative and positive torque spikes during the speed transition of the motor, specifically around 0.2s and 0.4s where there was a significant dip in torque below –40N-m. On the contrary, the ANN controller exhibited smaller torque ripples with smoother transitions and smaller peak values although some brief torque spike existed in the ANN response during rapid speed increase (around 0.6s and 0.8s). However, these spikes were more controllable and had fewer oscillations than those experienced by the PI controller. All things considered, the ANN controller offered improved dynamic performance relative to the conventional PI controller through reduced overshoot, a shorter settling time, and lower torque ripple as shown in Fig.15. These characteristics provide for a smoother running of the motor, reduce mechanical stress on the motor components, and improve overall efficiency which makes the ANN control strategy more attractive for use in high-performance electric vehicles

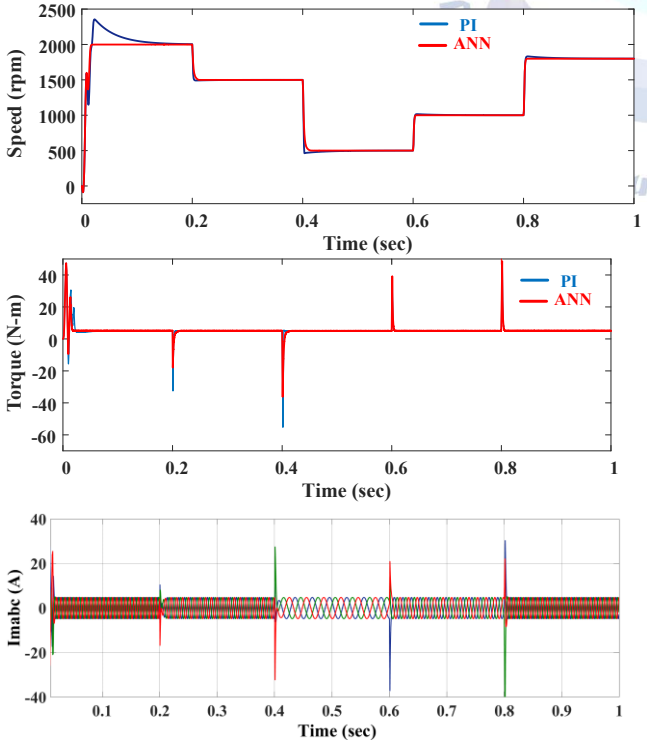

Fig. 15. Comparative simulation performance of PI and ANN controllers

X. CONCLUSION

The work has demonstrated a non-isolated single-inductor multiport dc-dc converter combined with a hybrid MPC-ANN controlled PMSM drive for use in electric vehicles. The proposed converter is able to combine solar PV and battery sources in order to provide flexibility in how much each source can contribute to the total power under both charge and discharge conditions. Compared to other converters that require many components and have a separate inductor for each output, the proposed converter was able to reduce component count and achieve a simple, low-cost design as well as allow for multiple regulated output voltages for traction and auxiliary loads. The ability to produce multiple output voltages allows for reliable and stable voltage regulation under changing input and load conditions. State space modeling demonstrates that the proposed converter will operate reliably in all possible operating modes. The addition of the VSI fed PMSM drive increases overall system performance due to the provision of a stable DC link voltage as well as increased efficiency of the drive. The proposed hybrid MPC-ANN controller has greatly improved PMSM speed control performance when compared to existing control methods. The proposed hybrid controller will provide a faster transient response, less overshoot and greater steady state accuracy than existing controllers while still being able to deal with system nonlinearities. Simulations performed using MATLAB/Simulink were used to verify that the proposed converter produces stable output voltages, manages energy efficiently from PV and battery systems, and tracks speed accurately with minimal torque ripple. In summary, the proposed system presents a robust and efficient means of managing electrical energy in an electric vehicle as well as controlling the motor, which makes it suitable for use in advanced electric vehicle applications.

Conflict of interest statement

Authors declare that they do not have any conflict of interest.

REFERENCES

[1] S. R. Khasim and C. Dhanamjayulu, ``Selection parameters and syn- thesis of multi-input converters for electric vehicles: An overview," Renew. Sustain. Energy Rev., vol. 141, May 2021, Art. no. 110804, doi: 10.1016/j.rser.2021.110804.

[2] P.-J. Liu, Y.-K. Lo, H.-J. Chiu, and Y.-J. Emery Chen, ``Dual-current pump module for transient improvement of step-down DC_DC converters,'' IEEE Trans. Power Electron., vol. 24, no. 4, pp. 985_990, Apr. 2009, doi: 10.1109/TPEL.2008.2010322.

[3] J. Macaulay and Z. Zhou, ``A fuzzy logical-based variable step size P&O MPPT algorithm for photovoltaic system,'' Energies, vol. 11, no. 6, p. 1340, May 2018, doi: 10.3390/en11061340.

[4] M. Dhananjaya, D. Ponuru, T. S. Babu, B. Aljafari, and H. H. Alhelou, ``A new multi-output DC_DC converter for electric vehicle application,'' IEEE Access, vol. 10, pp. 19072_19082, 2022.

[5] L. Wang, E. G. Collins, and H. Li, ``Optimal design and real- time control for energy management in electric vehicles,'' IEEE Trans. Veh. Technol., vol. 60, no. 4, pp. 1419_1429, May 2011, doi: 10.1109/TVT.2011.2122272.

[6] M. Zandi, A. Payman, J. P. Martin, S. Pierfederici, B. Davat, and F. Meibody-Tabar, ``Energy management of a fuel cell/supercapacitor/ battery power source for electric vehicular applications,'' IEEE Trans. Veh. Technol., vol. 60, no. 2, pp. 433_443, Nov. 2011, doi: 10.1109/TVT.2010.2091433.

[7] K. Suresh, C. Bharatiraja, N. Chellammal, M. Tariq, R. K. Chakrabortty, M. J. Ryan, and B. Alamri, ``Amultifunctional non-isolated dual input-dual output converter for electric vehicle applications,'' IEEE Access, vol. 9, pp. 64445_64460, 2021.

[8] S. R. Khasim and C. Dhanamjayulu, ``Design and implementation of asymmetrical multilevel inverter with reduced components and low voltage stress,'' IEEE Access, vol. 10, pp. 3495_3511, 2022, doi: 10.1109/ACCESS.2022.3140354.

[9] A. Ajami, H. Ardi, and A. Farakhor, ``A novel high step-up DC/DC converter based on integrating coupled inductor and switched- capacitor techniques for renewable energy applications,'' IEEE Trans. Power Electron., vol. 30, no. 8, pp. 4255_4263, Aug. 2015, doi: 10.1109/TPEL.2014.2360495.

[10] M. R. Banaei, H. Ardi, R. Alizadeh, and A. Farakhor, ``Non-isolated multi- input-single-output DC/DC converter for photovoltaic power generation systems,'' IET Power Electron., vol. 7, no. 11, pp. 2806_2816, Nov. 2014, doi: 10.1049/iet-pel.2013.0977.

[11] O. Hegazy, R. Barrero, J. Van Mierlo, P. Lataire, N. Omar, and T. Coosemans, ``An advanced power electronics interface for electric vehicles applications,'' IEEE Trans. Power Electron., vol. 28, no. 12, pp. 5508_5521, Dec. 2013, doi: 10.1109/TPEL.2013.2256469.

[12] C. Dhanamjayulu, S. Padmanaban, V. K. Ramachandaramurthy, J. B. Holm-Nielsen, and F. Blaabjerg, ``Design and implementation of multilevel inverters for electric vehicles,'' IEEE Access, vol. 9, pp. 317_338, 2021.

[13] Y. Cao and J. A. Abu Qahouq, ``Evaluation of bi-directional single-inductor multi-input battery system with state-of-charge balancing control,'' IET Power Electron., vol. 11, no. 13, pp. 2140_2150, Nov. 2018.

[14] S. R. Khasim, D. C, S. Padmanaban, J. B. Holm-Nielsen, and M. Mitolo, ``A novel asymmetrical 21-level inverter for solar PV energy system with reduced switch count,'' IEEE Access, vol. 9, pp. 11761_11775, 2021, doi: 10.1109/ACCESS.2021.3051039.

[15] Li, T.; Sun, X.; Lei, G.; Yang, Z.; Guo, Y.; Zhu, J. Finite-control-set model predictive control of permanent magnet synchronous motor drive systems—An overview. IEEE/CAA J. Autom. Sinica 2022, 9, 2087–2105.

[16] Faiz, J.; Mohseni-Zonoozi, S.H. A novel technique for estimation and control of stator flux of a salient-pole PMSM in DTC method based on MTPF. IEEE Trans. Ind. Electron. 2003, 50, 262–271.

[17] G. McClone, A. Ghosh, A. Khurram, B. Washom, and J. Kleissl, "Hybrid machine learning forecasting for online MPC of work place electric vehicle charging," IEEE Trans. Smart Grid, vol. 15, no. 2, pp. 1891–1901, Mar. 2024.

[18] B. Adineh, M. R. Habibi, A. N. Akpolat, and F. Blaabjerg, "Sensorless voltage estimation for total harmonic distortion calculation using artificial neural networks in microgrids," IEEE Trans. Circuits Syst. II, Exp. Briefs, vol. 68, no. 7, pp. 2583–2587, Jul. 2021.

[19] Z. J. Lee et al., "Adaptive charging networks: A framework for smart electric vehicle charging," IEEE Trans. Smart Grid, vol. 12, no. 5, pp. 4339–4350, Sep. 2021.

[20] H. Tu, H. Feng, S. Srdic, and S. Lukic, "Extreme fast charging of electric vehicles: A technology overview," IEEE Trans. Transport. Electrific., vol. 5, no. 4, pp. 861–878, Dec. 2019.

[21] Li, Y.; Ruan, X.;Wang, Y.; Zhang, C. Hysteresis Voltage Prediction Control for Multilevel Converter in the Series-Form Switch-Linear Hybrid Envelope Tracking Power Supply. IEEE Trans. Power Electron. 2020, 35, 13663–13672.

[22] B. Adineh, M. R. Habibi, A. N. Akpolat, and F. Blaabjerg, "Sensorless voltage estimation for total harmonic distortion calculation using artificial neural networks in microgrids," IEEE Trans. Circuits Syst. II, Exp. Briefs, vol. 68, no. 7, pp. 2583–2587, Jul. 2021.